International Conference on Artificial Reality and Telexistence
Eurographics Symposium on Virtual Environments (2025)
J. A. Jorge and N. Sakata (Editors)

Projecting BRDF Materials using Polarimetric Normal Estimation

Sota Matsuno[1] and Toshiyuki Amano[1]

[1]Faculty of Systems Engineering, Wakayama University, Japan

Abstract

This study proposes a method based on Spatial Augmented Reality (SAR) technology to transform the perceived material of an object's surface by projecting imagery rendered from measured BRDF data. The core of this method lies in the non-contact estimation of the object's three-dimensional surface shape from images captured at four different polarization angles. Specifically, Stokes parameters are calculated from four polarized images, and a normal vector is derived for each pixel based on the resulting Angle of Linear Polarization (AoLP) and Degree of Linear Polarization (DoLP). Next, rendering is performed using the estimated normal map and a measured BRDF database. The resulting appearance of the target material is then projected onto the object via a projector-camera system. Experiments demonstrate the ability to change the material appearance of certain objects, such as plaster statues and plastic products. The significance of this research lies in demonstrating a new framework for presenting material appearance by combining shape estimation using polarization with physically based rendering.

1. Introduction

The appearance of physical objects in the real world, particularly their material appearance, plays a crucial role in various fields such as product design evaluation, digital archiving of cultural heritage, and entertainment. Spatial Augmented Reality (SAR) [BR05] offers a powerful paradigm for altering the appearance of objects without physical modification. This technology does not require personal devices like head-mounted displays, allowing multiple viewers to share the augmented reality space simultaneously.

Since the pioneering work of Shader Lamps [RWLB01], research has advanced beyond texture projection using radiometric compensation [GN04] to achieve more realistic material appearances, such as metallic gloss. Such data-driven rendering approaches rely on pre-measured reflectance models [MPBM03] or sophisticated measurement techniques [MSY07]. Specific proposals include the presentation of dynamic material appearance using pixel brightness optimization with multiple projectors [SSL*15], and the reproduction of complex BRDFs using real-time ray tracing [NKW20]. However, these optics-model-based methods require geometric information like normal directions as a model and necessitate dynamic tracking of the object for projection.

As an alternative, methods that do not use geometric models have been proposed, such as reproducing the appearance of objects with structural color [MA18] or anisotropic reflection [OA22] through reflection analysis and light-field projection using a multi-projector-camera system. While this approach achieves material appearance that changes with viewpoint, it still assumes the normal direction of the projection target's surface, making it unable to adaptively present materials on arbitrary shapes. To solve these problems, the introduction of Physically Based Rendering (PBR), which involves estimating normal directions and reflection properties, is essential.

To address these limitations, this paper proposes a novel SAR framework that integrates polarimetric normal estimation with PBR. Our core contribution is an appearance-control pipeline that first estimates surface normals from four polarization images captured at different angles. While recent work also leverages polarization for detailed shape and reflectance [IKN25], our work focuses on integrating this sensing technique into a complete framework to actively transform the perceived material appearance in an SAR context.

2. Physical Principles of Shape Estimation by Polarization

2.1. Mathematical Formulation of Polarization State

The polarization state of light is described by the Stokes vector, $\mathbf{S} = [S_0, S_1, S_2, S_3]^T$. In this study, we compute the parameters for linear polarization from four intensity images, $I_0, I_{45}, I_{90}, I_{135}$, captured by a polarization camera with its transmission axis at $0, 45, 90, 135[deg]$.

$$S_0 = I_0 + I_{90} \tag{1}$$

$$S_1 = I_0 - I_{90} \tag{2}$$

$$S_2 = I_{45} - I_{135} \tag{3}$$

From these Stokes parameters, the Angle of Linear Polarization (AoLP) ψ and the Degree of Linear Polarization (DoLP) ρ, which characterize the state of polarization, are obtained by the following equations. These serve as the fundamental observables for estimat-

DOI: 10.2312/egve.20251355

ing the surface normal.

$$\psi = (1/2)\arctan(S_2/S_1) \tag{4}$$

$$\rho = \sqrt{S_1^2 + S_2^2}/S_0 \tag{5}$$

2.2. Surface Normal Estimation from Polarization Information

The normal vector at each point on a surface is uniquely determined by two angles: the zenith angle θ (the tilt of the normal) and the azimuth angle ϕ (the orientation of the normal). These angles are estimated from the AoLP and DoLP.

2.2.1. Estimation of Azimuth Angle ϕ

In specular reflection, the polarization direction of the reflected light is perpendicular to the plane of incidence (the plane containing the incident ray, the reflected ray, and the normal vector). Therefore, there is always a phase difference of $\pi/2$ between the observed AoLP (ψ) and the normal's azimuth angle ϕ. This relationship, expressed by the following equation, allows for the direct estimation of the azimuth angle. This estimation is directly linked to physical laws and is relatively robust.

$$\phi = \psi + \pi/2 \tag{6}$$

2.2.2. Estimation of Zenith Angle θ

The estimation of the zenith angle θ is more complex. Physically, the DoLP is governed by the Fresnel equations, which depend on the surface's refractive index and the angle of incidence (equal to the zenith angle θ). This relationship creates two challenges: it can be ambiguous, as a single DoLP value may correspond to two different angles, and it requires prior knowledge of the refractive index. To avoid these complexities and prioritize computational simplicity and versatility, this study adopts a simplified linear model:

$$\theta = (\pi/2) \cdot \rho \tag{7}$$

This approximation is based on the physical tendency that the DoLP is 0 at a zenith angle of $0[deg]$ (normal incidence) and increases monotonically with the angle (at least up to Brewster's angle). This model does not require information about the refractive index and avoids the ambiguity problem, making it extremely easy to implement. However, it is merely a first-order approximation that ignores the physically rigorous relationship, thus imposing an inherent limit on the accuracy of the estimated zenith angle. This design choice is considered an intentional trade-off to obtain a reasonable proxy for the shape at a practical cost for the specific application of material appearance transformation, rather than aiming for perfect shape acquisition.

3. System Design and Implementation

The system flowchart is shown in Figure 1. The process is executed as a pipeline consisting of surface normal estimation, physically based rendering, and geometrically corrected projection.

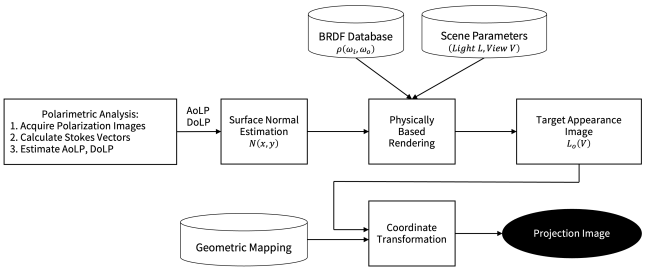

Figure 1: *Processing Flow*

3.1. Stage 1: Surface Normal Estimation

The first stage of the process is the estimation of the target's surface normals. First, four intensity images ($I_0, I_{45}, I_{90}, I_{135}$) are acquired from a polarization camera. Next, Stokes parameters are calculated to generate AoLP and DoLP maps. After applying a median filter for noise reduction, the azimuth angle ϕ is derived from the smoothed AoLP map, and the zenith angle θ is derived from the DoLP map using the linear approximation model. Finally, these azimuth and zenith angle maps are converted to a Cartesian coordinate system, completing the 3-channel normal map used for the subsequent rendering stage.

3.2. Stage 2: Physically Based Rendering with Measured BRDF

In the second stage, physically based rendering is performed using the estimated normal map. The MERL BRDF Database [MPBM03] is used, which contains measured reflectance data for a vast number of incident and outgoing direction combinations. It is parameterized in the computationally efficient half-vector coordinate system $(\theta_h, \theta_d, \phi_d)$. Therefore, the rendering process requires converting world-coordinate vectors (normal $\mathbf{n}$, light direction $\mathbf{l}$, view direction $\mathbf{v}$) for each pixel into this half-vector coordinate system to look up the database.

3.2.1. Rendering Equation

The fundamental reflection equation for physically based rendering is expressed as follows [PJH16]:

$$L_o(\mathbf{v}) = \int_\Omega f_r(\mathbf{l}, \mathbf{v}) L_i(\mathbf{l})(\mathbf{n} \cdot \mathbf{l}) d\mathbf{l} \tag{8}$$

As this system assumes a single directional light source (the projector), this integral is simplified to a direct product for the outgoing radiance L_o:

$$L_o = f_r(\mathbf{l}, \mathbf{v}) \cdot C_{\text{light}} \cdot \max(0, \mathbf{n} \cdot \mathbf{l}) \tag{9}$$

where f_r is the BRDF, $\mathbf{l}$ and $\mathbf{v}$ are the light and view vectors, $\mathbf{n}$ is the surface normal, and C_{light} represents the light source's color and intensity.

3.2.2. Rendering Process

Each pixel is rendered using the estimated normal vector, and the light and view vectors determined by the scene configuration. From these vectors, the parameters for the half-vector coordinate system

are calculated, and the MERL BRDF Database is referenced to obtain the RGB reflectance values. The final color of the pixel is determined by multiplying this reflectance by the light source color and the dot product of the normal and light direction.

3.2.3. Radiometric Considerations

This system simplifies radiometric compensation and currently does not account for spatial non-uniformities in the object's original color or texture. It is limited to multiplying the entire rendered image by a single brightness correction factor to adjust the visibility of the projected result according to the projector's brightness and the object's surface (or physical) reflectance.

3.3. Stage 3: Geometrically Corrected Projection

To align the rendered image with the target object, we pre-calibrate the geometric mapping between the camera and projector using standard Gray-code structured light. This process generates a lookup map (Fig. 2) to warp the rendered image before projection.

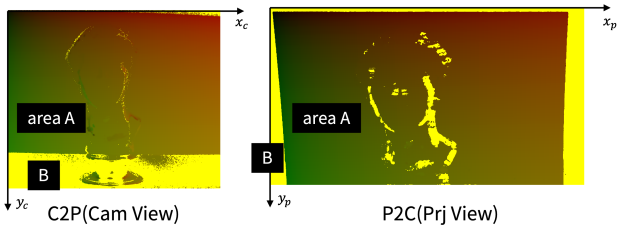

Figure 2: *Pixel map showing geometric correspondence between the projector and camera. R, G channels indicate x, y coordinates, respectively. Correspondence exists in area A but not in area B.*

4. Results and Discussion

The projector-camera system used in this study is shown in Figure 3. The hardware consists of a DLP projector (Vivitek QUMI Q6-BK), whose projection light is unpolarized, and a polarization camera (FLIR Blackfly S BFS-U3-51S5P) capable of capturing polarized images in four directions $(0, 45, 90, 135[deg])$ simultaneously. The baseline (distance between the projector lens and the camera lens) was 50mm, and the distance from the projector lens to the target object was 1000mm.

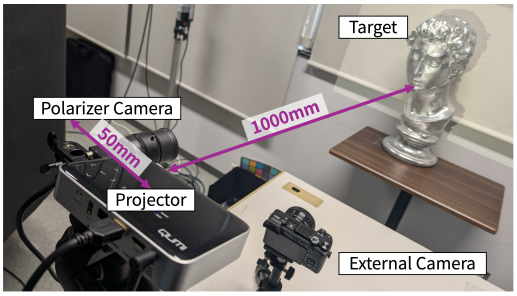

Figure 3: *Hardware configuration of the experimental system*

Figure 4 shows the experimental results of applying our method to objects of various shapes and materials, as captured by an external camera. To enhance visibility for projection, all BRDF renderings (including the target material samples shown in the top row) were processed with a boosted gain. For predominantly diffuse objects such as the plaster statue and the helmet (Fig. 4 (b, c)), a small amount of surface gloss allowed polarization-based normal estimation. Projecting a metallic material created natural highlights along the object's curves, changing its perceived material. On the other hand, application to the metallic bust (Fig. 4 (a)), which originally has strong specular reflection, and the earthenware (Fig. 4 (d)), whose surface irregularities cause nearly Lambertian reflection, proved difficult.

4.1. Evaluation and Discussion with Luminance Profiles

To quantitatively evaluate the material reproduction, we performed a correlation analysis of luminance profiles. This method compares the relationships among the estimated object shape, the theoretical luminance predicted by the BRDF model, and the actual measured luminance from the projection.

1. **Geometric Proxy Profile:** The angle θ_h between the normal vector **n** and the half-vector **H**, obtained from the normal map. Plotted as $1 - \mathrm{norm}(\theta_h)$ to visually align with luminance peaks.
2. **BRDF Luminance Profile:** The theoretical luminance value calculated by referencing the MERL BRDF database with the normal information for each point.
3. **Measured Luminance Profile:** The polarization-independent luminance value S_0 calculated from two captured polarized images (I_0, I_{90}) of the actual projection onto the object.

These three profiles are normalized to $[0, 1]$ and plotted on a single graph. Figure 6 shows excerpts from the analysis when applying optically contrasting materials ('chrome' and 'red-plastic').

4.1.1. Uncertainty in Shape Estimation and Its Impact

The foundation of this method is normal estimation via polarization, and its accuracy directly impacts rendering quality. In particular, the linear approximation model (Eq. 7) for the zenith angle is a deliberate trade-off, sacrificing physical rigor for versatility. This approach is successful for objects with smooth surfaces like the plaster statue and the helmet, where the AoLP map smoothly reflects the object's curvature, enabling normal estimation (Fig. 6 (b2, c2)).

Despite the estimation process being sensitive to noise (Fig. 5), the final results (Fig. 4) successfully reproduce the material appearance and illumination gradients, similar to the rendered samples, except for (d). This robustness is particularly evident for (b) and (c), which are predominantly diffuse. As discussed in the following section on modulation (Sec. 4.1.2), their intrinsic surface properties act as a low-pass filter, smoothing any sharp highlights or high-frequency noise from the projection. This interaction effectively masks the underlying errors from the normal estimation, leading to a visually stable and plausible result.

4.1.2. Surface interaction on the Object Surface

Another factor is the interaction between the projected illumination and the surface, including interreflections in concave regions and

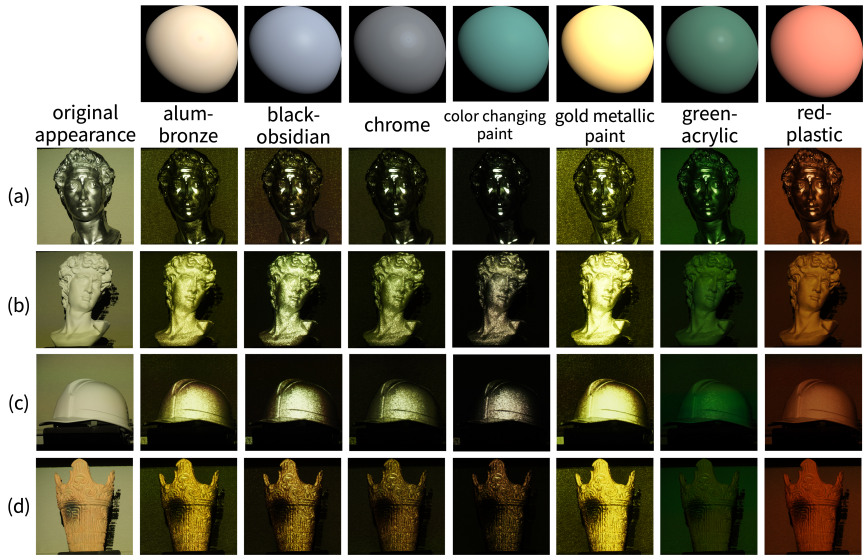

Figure 4: *Projection results captured by an external camera. (a) Metallic bust (specular object), (b) Plaster statue (diffuse object), (c) Helmet (smooth plastic with diffuse and specular reflection), (d) Earthenware (diffuse object with complex surface geometry)*

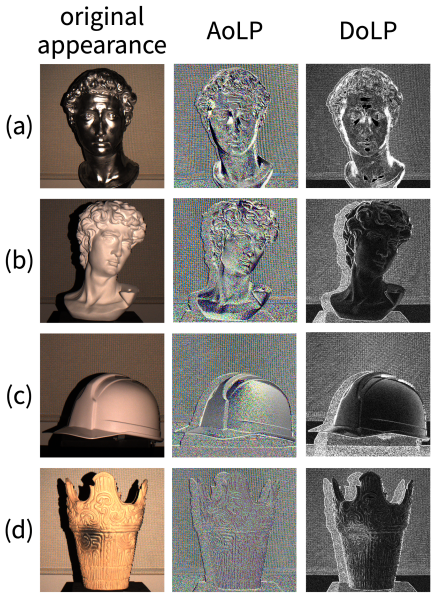

Figure 5: *AoLP and DoLP maps*

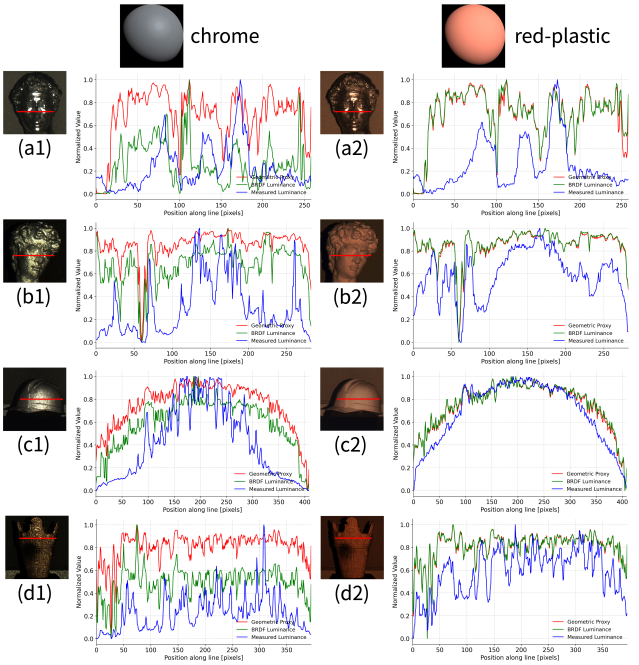

Figure 6: *Illumination profiles: Geometric Proxy Profile (red), BRDF Luminance Profile (green), and Measured Luminance Profile (blue). Theoretically, for a smooth Lambertian surface, the measured profile should coincide with the BRDF data, as shown in (c2).*

spatially non-uniform reflection distributions arising from specular components. Consequently, the measured luminance profile (blue) inevitably reflects the modulation of the projected light by the object's intrinsic reflectance characteristics. Interreflections introduce errors in normal estimation, leading to noticeable illumination drops in the measured luminance, as shown in Fig. 6 (b1, b2). The effect of specular reflection is particularly evident on the metallic bust (Fig. 6 (a1, a2)), where a significant discrepancy appears between the theoretical target profile (green) and the measured profile (blue). This discrepancy arises because the surface illumination distribution is modulated by specular reflection, producing illumination peaks in addition to the Lambertian component. These peaks often cause luminance saturation and a loss of gradation. These findings indicate that the proposed method performs best on surfaces exhibiting spatially uniform and mainly diffuse reflectance, where interreflections and specular modulation effects are minimized.

5. Conclusion

In this study, we demonstrated a SAR-based framework for projecting material appearances using measured BRDF data and polarimetric normal estimation.

Future work includes replacing the simplified linear model (Eq. 7) with a more physically rigorous solution, such as iterative optimization against the Fresnel equations, to resolve the zenith angle ambiguity. Additionally, incorporating radiometric calibration would compensate for the object's base material.

Acknowledgements This work was supported by JSPS KAKENHI Grant Numbers JP24K02979, JP25H01886.

References

[BR05] BIMBER O., RASKAR R.: *Spatial Augmented Reality: Merging Real and Virtual Worlds*. A K Peters, 2005. 1

[GN04] GROSSBERG M. D., NAYAR S. K.: Modeling the Space of Camera Response Functions. *IEEE Transactions on Pattern Analysis and Machine Intelligence 26*, 10 (2004), 1272–1282. 1

[IKN25] ICHIKAWA T., KAWAHARA R., NISHINO K.: Single-Shot Shape and Reflectance with Spatial Polarization Multiplexing. *arXiv preprint arXiv:2504.13177* (2025). arXiv:2504.13177, doi:10.48550/arXiv.2504.13177. 1

[MA18] MURAKAMI K., AMANO T.: Materiality Manipulation by Light-Field Projection from Reflectance Analysis. In *Proceedings of the International Conference on Artificial Reality and Telexistence and Eurographics Symposium on Virtual Environments (ICAT-EGVE)* (2018). 1

[MPBM03] MATUSIK W., PFISTER H., BRAND M., MCMILLAN L.: A data-driven reflectance model. *ACM Transactions on Graphics 22*, 3 (jul 2003), 759–769. 1, 2

[MSY07] MUKAIGAWA Y., SUMINO K., YAGI Y.: Multiplexed illumination for measuring BRDF using an ellipsoidal mirror and a projector. In *Computer Vision – ACCV 2007* (Berlin, Heidelberg, 2007), Yagi Y., Kang S. B., Kweon I. S., Zha H., (Eds.), vol. 4844 of *Lecture Notes in Computer Science*, Springer, pp. 306–319. doi:10.1007/978-3-540-76390-1_25. 1

[NKW20] NOMOTO T., KOISHIHARA R., WATANABE Y.: Realistic Dynamic Projection Mapping Using Real-Time Ray Tracing. In *SIGGRAPH 2020 Emerging Technologies* (2020). 1

[OA22] OHSUMI S., AMANO T.: Manipulation of Anisotropic Reflections Based on Optical Models Using Multiple Projectors. In *CEUR Workshop Proceedings* (2022), vol. 3330. 1

[PJH16] PHARR M., JAKOB W., HUMPHREYS G.: *Physically Based Rendering: From Theory to Implementation*, 3rd ed. Morgan Kaufmann, 2016. 2

[RWLB01] RASKAR R., WELCH G., LOW K.-L., BANDYOPADHYAY D.: Shader Lamps: Animating Real Objects with Image-Based Illumination. In *Proceedings of the 12th Eurographics Workshop on Rendering* (2001). 1

[SSL*15] SIEGL C., SRA M., LI W., BIMBER O., BIRSAK M.: Real-Time Pixel Luminance Optimization for Dynamic Multi-Projection Mapping. *ACM Transactions on Graphics (TOG) 34*, 6 (2015), 1–11. 1